Comparison of Winding Concepts for Bearingless Pumps

K. Raggl, J. W. Kolar
Power Electronic Systems Laboratory
ETH Zurich
8092 Zurich, Switzerland
Email: raggl@lem.ee.ethz.ch

T. Nussbaumer
Levitronix GmbH
Technoparkstrasse 1
8005 Zurich, Switzerland
Email: nussbaumer@levitronix.com

***Abstract*— Bearingless slice motors as employed in semiconductor, pharmaceutical and medical industry perform magnetic levitation by radial bearing forces and rotation by tangential forces. This requires bearing and drive windings, which can be realized as separate bearing and drive coils or as identical, concentrated coils on the stator claws. In this paper, a detailed comparison between these two winding concepts is undertaken, where the coil losses, the coil volume, the power electronics requirements and the achievable rotation speed are evaluated. Furthermore, practical features such as control complexity, cabling effort and manufacturability are taken into account. Finally, the trade-off between losses, volume and realization effort will be discussed in order to give a guideline for the selection of the appropriate winding concept for a specific application of a bearingless pump.**

I. Introduction

Bearingless motors have been extensively investigated during the past years and have been employed successfully in high purity environments (e.g. in semiconductor, pharmaceutical and medical industry e.g. as pumps or mixers) due to their great variety of benefits such as non–contact bearing capability and the lack of mechanical wearing, lubricants and seals [1], [2], [3].

However, new applications require a further optimization of the pump systems, i.e. the maximization of the hydraulic pump pressure while minimizing the pump volume, the power losses and the costs of the pump system [4]. Within this optimization, a crucial element that determines the performance of the pump system is the motor part. Here, the required bearing and drive forces can be generated for the same mechanical motor setup by different winding concepts of the bearing and drive coils. As will be shown in this paper, this may have an influence on the resulting losses, the coil volume and the pump performance.

The comparison is based on a pump system with a diametrically, one pole pair rotor (cf. Fig. 1). The optimum pole pair number for the drive system ($p_d = 1$) and the bearing system ($p_b = 2$) for this setup has been discussed extensively in literature [5], [6], [7], [8]. Furthermore, it has been found that for achieving full control freedom for the drive and bearing system at least eight stator claws are needed [5]. With this, the motor setup as shown in Fig. 1 is defined for the comparison in this paper.

Fig. 2 shows the two winding concepts that will be analysed in the following (two of the eight stator claws are shown). For the conventional setup (cf. Fig. 2(a)) two separate coils are used to impress the bearing and the drive forces separately [1], [2], [3] where each bearing coil is wound over a claw and each drive coil is wound over two claws.

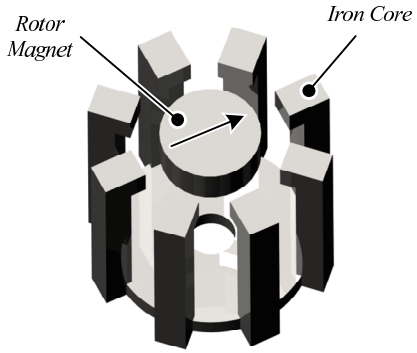

Fig. 1: Basic setup of a bearingless slice motor for a centrifugal pump with a diametrically magnetized rotor

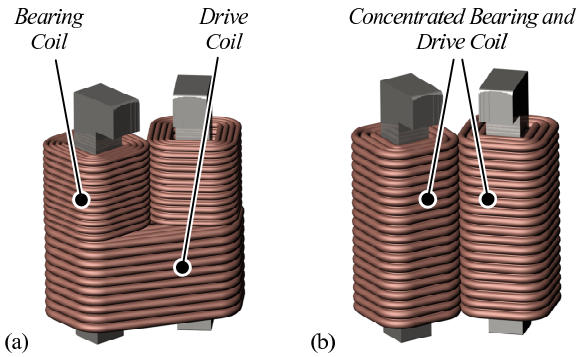

Fig. 2: Winding concepts for the bearingless pump — separated coils (a) and concentrated coils (b) (detailed view on two of the eight stator claws)

An alternative way is to apply only one coil on each claw (cf. Fig. 2(b)) as it is done eg. in 1–phase bearingless motor configurations [9], [10]. This concepts results in easier assembly and therefore lower price but on the other hand in a bigger control and power electronics effort since each current has to be calculated and impressed in each coil separately.

The discussion of these two winding concepts is based on the following assumptions:

- Same motor setup (iron circuit, rotor magnet size and magnetization)
- Same required bearing force and torque for both concepts
- Same max. allowable current density
- Same winding factor

After a short explication of the generation of the bearing and drive forces in section II, in the subsequent sections the

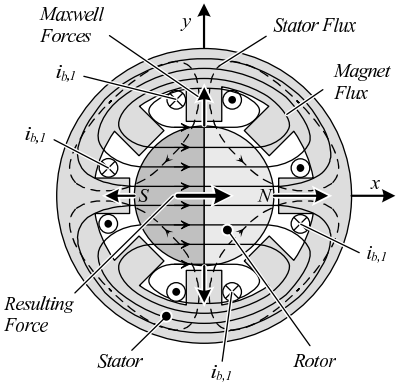

Fig. 3: Maxwell Force generation in magnet direction

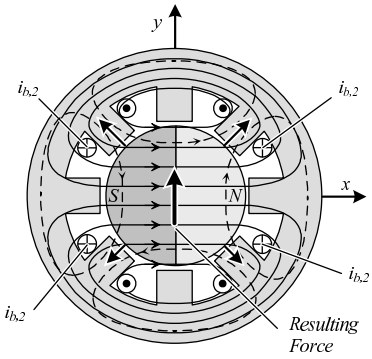

Fig. 4: Maxwell Force generation perpendicular to magnet direction

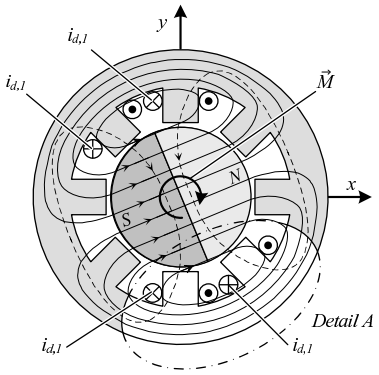

Fig. 5: Torque generation with one phase — the second phase is rotated by 90 deg

detailed comparison is performed, i.e.:

- Section III: Copper losses
- Section IV: Coil volume
- Section V: Power electronics requirements
- Section VI: Maximum achievable rotation speed

Finally, experimental measurements on an existing pump system with separated coils verify the correctness of the considerations in section VII.

II. Force generation

In this section, the generation of the bearing and drive forces is explained for the two winding concepts based on the motor setup at hand (cf. Fig. 1). The fundamentals are essential for the understanding of the comparison in the subsequent sections.

The principle of the bearing force generation is shown in Fig. 3 for resulting forces in magnet direction and in Fig. 4 for resulting forces perpendicular to magnet direction. For sake of clearness, only Maxwell–forces are shown in these figures. The magnetized rotor is impressing a magnetic field into the stator (solid lines in Fig. 3) directed from the magnet north pole through the stator to the magnet south pole. By applying a current $i_{b,1}$ in the shown coils a superposed magnetic field (dashed lines) is generated. This field, impressed by the coils, leads to an attenuation of the permanent magnet field in the left air gap and a reinforcement of the magnet field in the right air gap. According to the Maxwell–equations these two magnetic fields causes forces on the magnet surface directed from the medium with higher permeability to the medium with lower permeability, which is proportional to the air gap field $\vec{F} \propto \vec{B}$. With the shown current direction of $i_{b,1}$ in Fig. 3 a resulting force in positive x–direction is built up.

Additionally, forces based on the Lorentz–equations appear in this setup [5], [11]. As generally known, the force on a conductor, in which a current is flowing and which is positioned in a magnetic field, is given by $\vec{F} = i \cdot (\vec{l} \times \vec{B})$. The appearing Lorentz–forces are superposed to the Maxwell–forces and directed in the same direction.

Fig. 4 shows the bearing force generation perpendicular to the magnet direction. In this case, Maxwell– and Lorentz–forces are superposed again and with currents $i_{b,2}$ flowing in the direction shown in Fig. 4 a resulting force in positive y–direction is built up.

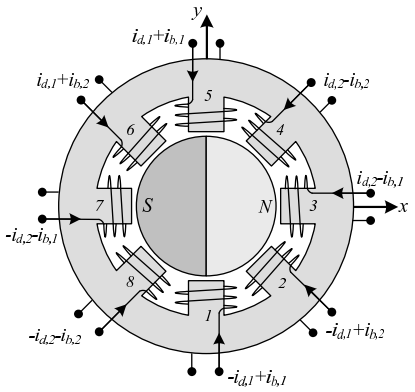

Fig. 6: Needed currents in each coil in case of concentrated coils.

With this application, it is possible to generate forces in x– and y–direction independent of the angular rotor position.

The torque generation due to one drive phase is depicted in Fig. 5. The impressed current $i_{d,1}$ in the shown coils leads to a magnetic field orthographic to the magnetic rotor field for this specific angular rotor position. This leads to a resulting torque on the rotor as shown in Fig. 5. By applying a sinusoidal current $i_{d,2}$ with a phase shift of $90\,^\circ$ with respect to $i_{d,1}$ on the four remaining stator claws in an analogous manner a constant torque can be built up.

A. Separated Coils

Since the same currents (e.g. $i_{b,1}$ in Fig. 3 and $i_{b,2}$ in Fig. 4) are flowing through the shown coils, they can be directly connected in series. Therefore, only two bearing phases are needed to ensure levitation in x– and y–direction. Another speciality of that winding configuration is that the appearing induced voltage in the bearing phases is eliminated due to the symmetry. This leads to a higher available coil voltage and hence to an increased bearing dynamics.

The drive coils shown in Fig. 5 can be connected in series too, hence in total four independent full–bridges are needed to generate autonomous forces in x– and y–direction and a torque in z–direction for this coil setup. Since always two neighbored coils carry the same current, the drive windings can be wound over two claws, as it is shown in Fig. 2. As it

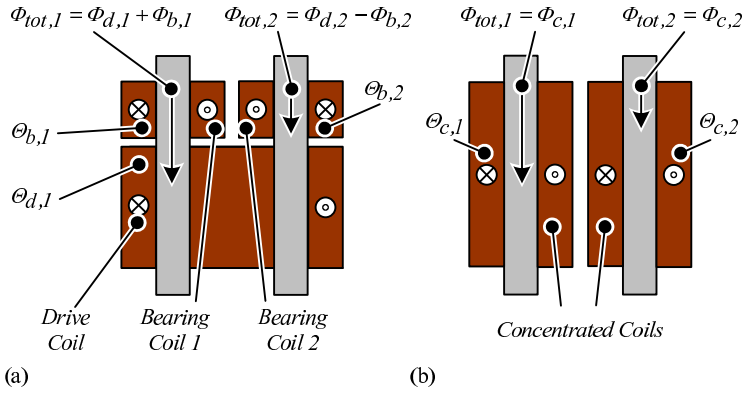

Fig. 7: Separated (a) and concentrated (b) winding concepts for a bearingless slice motor with eight claws. For better visibility only two of the eight stator claws are shown.

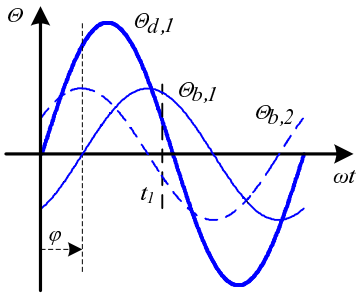

Fig. 8: General curves of ampere-turns in bearing and drive with a global force acting on the rotor

will be shown later (cf. section III-B) this slightly reduces the average winding length and therefore the copper losses of the separated coils.

B. Concentrated coils

Out of the Figures 3, 4 and 5 the needed currents per coil can be ascertained. The resulting situation is shown in Fig. 6. One can see easily that in case of concentrated coils a simplification by connecting two or more coils in series is not possible anymore due to a different current needed in each coil. Consequently, eight full–bridges are needed in case of concentrated coils to ensure the same performance. However, this does not necessarily mean a disadvantage. The power electronics effort will be evaluated separately in section V.

III. Copper Losses

For the subsequent analysis of the copper losses in the bearing and drive coils we exemplary look at one stator claw pair (cf. *Detail A* in Fig. 5 and stator claws 1 and 2 in Fig. 6). The situation at the claws 3–8 can be analysed in an analogous way by symmetry considerations. In Fig. 7 the magnetic flux generation in these claws through the bearing and drive ampere–turns is illustrated for the case of separated (cf. Fig. 7(a)) and concentrated (cf. Fig. 7(b)) coils.

Due to the winding arrangement of the separated coils [1], the flux phase difference between two neighbored bearing coils (cf. Fig. 8) has to be 90° to ensure levitation [5]. As a matter of fact, the needed ampere–turns in the bearing have the same frequency as the drive ampere–turns. However, in case of a centrifugal pump, a steady asymmetric force is acting on the rotor directed to the hydraulic outlet of the pump due to a pressure loss at the outlet, which causes a load angle φ between the drive and bearing ampere–turns (cf. Fig 8). Exemplarily, we are looking now at a typical operation state at $t = t_1$. Here, the impressed magnetic flux of the bearing coil is operating against the impressed flux of the drive coil in the right iron claw (Fig. 7(a)). Therefore, the resulting magnetic flux $\Phi_{tot,2}$ in that claw is reduced due to counteraction of the individual magnetic fluxes. Obviously, in the case of concentrated coils (Fig. 7(b)) the same resulting flux $\Phi_{tot,2}$ in the right claw can be built up by less impressed current, wherefore lower copper losses occur in this setup for the same ampere–turns. This loss reduction will be quantified in the following.

A. General loss reduction

Generally, the copper losses can be written as

$$P_{cu} = R \cdot I_{rms}^2 \tag{1}$$

and can be transformed with $R = N \cdot \frac{\rho_{cu}\, l_m}{A_{cu}}$ and $\Theta_{rms} = N \cdot I_{rms}$ to

$$P_{cu}(\Theta) = N^2 \cdot \frac{\rho_{cu}\, l_m}{A_{tot}\, k_f} \cdot \frac{\Theta_{rms}^2}{N^2} = \frac{\rho_{cu}\, l_m}{A_{tot}\, k_f} \cdot \Theta_{rms}^2 \tag{2}$$

dependent on the *rms* value of the impressed ampere–turns Θ_{rms}. In (2) k_f means the winding factor, A_{tot} the whole coil cross area, A_{cu} the wire cross area, ρ_{cu} the copper density, l_m the average winding length per claw and N the winding number. The wire cross area is given by

$$A_{cu} = \frac{A_{tot} \cdot k_f}{N}. \tag{3}$$

With this, the needed ampere–turns

$$\begin{bmatrix} \Theta_{b,1} \\ \Theta_{b,2} \\ \Theta_{d,1} \\ \Theta_{d,2} \end{bmatrix} = \begin{bmatrix} \hat{\Theta}_b \cdot \sin(\omega t - \varphi) \\ \hat{\Theta}_b \cdot \cos(\omega t - \varphi) \\ \hat{\Theta}_d \cdot \sin(\omega t) \\ \hat{\Theta}_d \cdot \cos(\omega t) \end{bmatrix} \tag{4}$$

and (2) the copper losses can be calculated for each claw and coil separately in case of separated coils. The total copper losses for all coils are given by

$$P_s = 4{\cdot}P_{cu}(\Theta_{b,1}){+}4{\cdot}P_{cu}(\Theta_{b,2}){+}4{\cdot}P_{cu}(\Theta_{d,1}){+}4{\cdot}P_{cu}(\Theta_{d,2}). \tag{5}$$

In (5) the same average winding length l_m for drive and bearing coils has been assumed, i.e. the drive windings are wound around the stator claws individually in order to simplify the calculations in the first instant. By winding the drive coils around two stator claws the average winding length can be reduced by a geometry dependent factor k_{lm}. The influence of this factor on the copper losses will be analysed separately in section III-B.

In case of concentrated coils the needed ampere–turns per claw can be written as (cf. Fig. 6)

$$\begin{bmatrix} \Theta_{c,1} \\ \Theta_{c,2} \\ \Theta_{c,3} \\ \Theta_{c,4} \\ \Theta_{c,5} \\ \Theta_{c,6} \\ \Theta_{c,7} \\ \Theta_{c,8} \end{bmatrix} = \begin{bmatrix} \Theta_{b,1} - \Theta_{d,1} \\ \Theta_{b,2} - \Theta_{d,1} \\ -\Theta_{b,1} + \Theta_{d,2} \\ -\Theta_{b,2} + \Theta_{d,2} \\ \Theta_{b,1} + \Theta_{d,1} \\ \Theta_{b,2} + \Theta_{d,1} \\ -\Theta_{b,1} - \Theta_{d,2} \\ -\Theta_{b,2} - \Theta_{d,2} \end{bmatrix}. \tag{6}$$

The resulting copper losses are given by

$$P_c = \sum_{i=1}^{8} P_{cu}(\Theta_{c,i}) \tag{7}$$

with (2),(4) and (6). By calculating the copper losses P_s and P_c the loss reduction by implementing concentrated coils is derived by

$$\frac{P_c}{P_s} = \frac{\hat{\Theta}_b^2 + \hat{\Theta}_d^2}{\left(\hat{\Theta}_b + \hat{\Theta}_d\right)^2} \tag{8}$$

Equation (8) is valid under the assumption of the same current density for the separated bearing and drive coils

$$J_{s,rms} = \frac{\Theta_{b,rms}}{A_b} = \frac{\Theta_{d,rms}}{A_d} \tag{9}$$

and the assumption that the total coil volumes (i.e. cross areas) are the same for the separated and the concentrated setup:

$$A_c = A_d + A_b. \tag{10}$$

With this assumption in (10) it becomes clear, that the loss reduction for the concentrated coils is achieved through a lower current density $J_{c,rms} < J_{s,rms}$. This fact can also be utilized for a volume reduction as will be discussed separately in section IV. However, the results in this section are based on the equality of the coil volumes (10).

An interesting result is the independence of the copper loss reduction on the load angle φ. While the individual losses of claw pairs (cf. Fig. 7) show a dependency on φ, this dependency disappears by summation of the losses of all coils.

The calculated copper loss ratio is shown in Fig. 9 (solid line with $k_{lm} = 1$) with dependency on the ampere–turns ratio $\hat{\Theta}_d/\hat{\Theta}_b$. One can see that there is a maximum loss reduction of about $50\,\%$ at an ampere–turn ratio of $\hat{\Theta}_d/\hat{\Theta}_b = 1$. The ampere–turn ratio $\hat{\Theta}_d/\hat{\Theta}_b$ is dependent on the operating point and is typically in the range of 2–3. In this range a copper loss reduction of about $40\,\%$ is possible. A realistic value of improvement will be around $30\,\%$ due to the fact that non–sinusoidal, non–repetitive forces will always be present in the system to a certain extent, e.g. due to noise in the sensor signals.

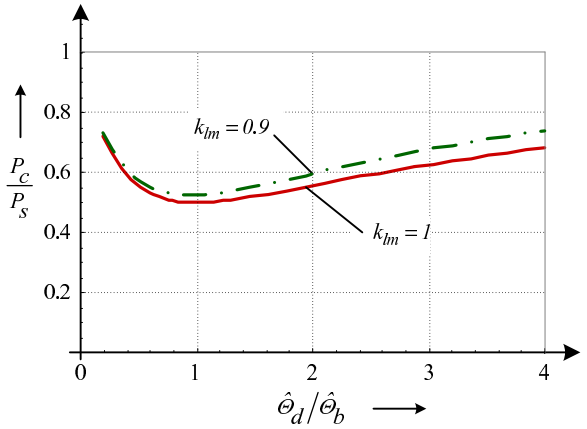

Fig. 9: Copper loss ratio P_c/P_s over ampere–turn ratio. The solid line indicates the losses for $k_{lm} = 1$ the chain dotted line for $k_{lm} = 0.9$

B. Influence of the average winding length factor

Due to the fact that two neighbored drive coils can be combined in case of separated coils (cf. Fig. 7) the average winding length and thus the resulting copper losses can be reduced. This amount of reduction will be calculated in the following. Based on the geometry shown in Fig. 10 the lengths

$$l_1 = \frac{1}{4}\pi\left(\sqrt{2}\,b_c + \sqrt{\left(2-\sqrt{2}\right)\,r_c^2}\right) \tag{11}$$

and

$$l_2 = \sqrt{\left(2-\sqrt{2}\right)\,r_c^2}. \tag{12}$$

can be calculated. Here it is assumed that the available space between the stator claws is completely used, i.e. filled with coils as depicted in Fig. 10. The average winding length $l_{m,2}$ of a combined drive coil is therefore given by

$$l_{m,2} = 2\,l_1 + 2\,l_2 = \frac{b_c\,\pi}{\sqrt{2}} + \frac{1}{2}(4+\pi)\sqrt{\left(2-\sqrt{2}\right)\,r_c^2}. \tag{13}$$

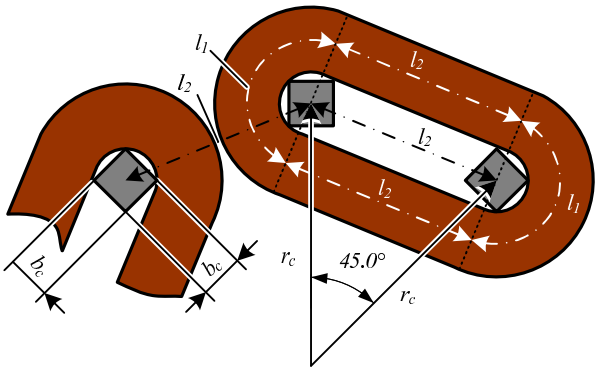

Fig. 10: Geometries for the calculation of the average winding length of a combined drive coil in case of separated coils.

If all drive coils were separately wound around the claws, the average winding length of one drive coil would be

$$l_{m,1} = \pi\left(\sqrt{2}\,b_c + \sqrt{\left(2-\sqrt{2}\right)\,r_c^2}\right). \tag{14}$$

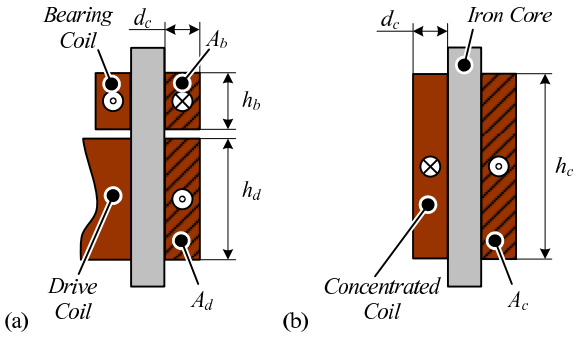

Fig. 11: Coil dimensions

Hence, the average winding length reduction by combining the coils can be written to

$$\frac{l_{m,2}}{l_{m,1}} = k_{lm} = \frac{\sqrt{2}\,\pi\,b_c/r_c + (4+\pi)\,\sqrt{(2-\sqrt{2})}}{2\,\pi\left(\sqrt{2}\,b_c/r_c + \sqrt{(2-\sqrt{2})}.\right)} \tag{15}$$

Usually, the factor b_c/r_c is in the range of $0.3 - 0.45$ resulting in a typical value of $k_{lm} = 0.9$. This leads to a slight decrease of the copper losses of the separated coils when taking the average winding length reduction k_{lm} into consideration in (8). The corrected copper loss ratio can be calculated by

$$\frac{P_c}{P_s} = \frac{\hat{\Theta}_b^2 + \hat{\Theta}_d^2}{\left(\hat{\Theta}_b + \hat{\Theta}_d\right)\left(\hat{\Theta}_b + k_{lm}\,\hat{\Theta}_d\right)}. \tag{16}$$

Fig. 9 shows the copper loss ratios for $k_{lm} = 1$ and $k_{lm} = 0.9$. It can be seen that the factor k_{lm} for a realistic value of $k_{lm} = 0.9$ reduces the copper loss improvement of the concentrated coils by approximately $5\,\%$.

IV. Coil Volume

The previous section was based on the same iron circuit configuration, which leads to the same total coil volume (resp. total coil area $A_c = A_d + A_b$, cf. Fig. 11). Hence, the resulting current density for concentrated coils was lower in some coils causing the before mentioned loss reduction. Releasing the constraint of fixed iron circuit and dimensions may lead to a smaller coil volume in case of concentrated coils as will be shown in the following.

The current densities in the concentrated coils can be calculated with

$$J_{c,i,rms} = \frac{\Theta_{c,i,rms}}{h_c\,d_c}. \tag{17}$$

Using (6) and (4) for evaluating (17) leads to dependencies of the current densities on the load angle φ, i.e. for a certain load angle different current densities $J_{\Theta,c,i,rms}$ will occur in the coils. Exemplarily, in Fig. 12 (lower graph) it is illustrated, how the coil volume could be reduced if only the maximum current density of coil 1 would be kept, i.e. $J_{c,1,rms} = J_{max}$. However, as can be seen in the upper graph, in the area of the volume decrease the current densities in the other coils increase drastically $J_{c,i,rms} > J_{max}$, which can lead to local overheating and should be avoided generally (area of local current density exceedance in Fig. 12).

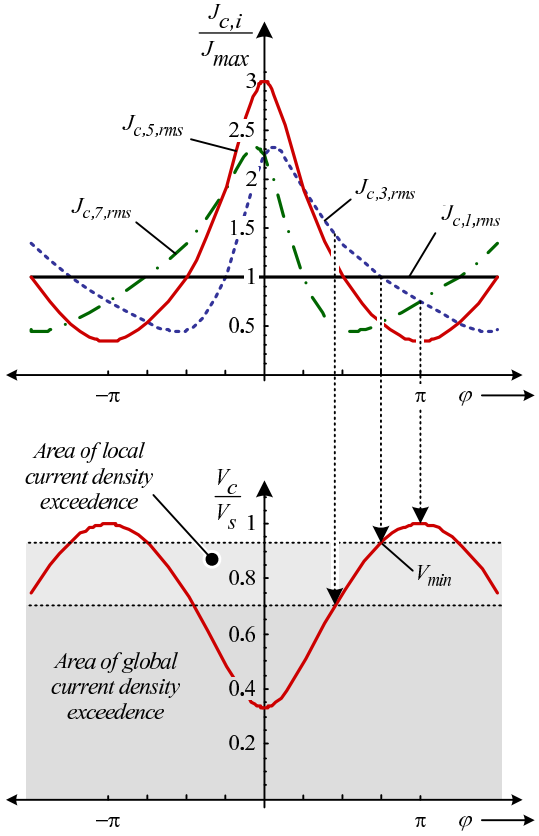

Fig. 12: Local current densities in the concentrated coils for the condition $J_{c,1,rms} = J_{max}$ (upper curve); resulting coil volume reduction for that condition in dependency on the load angle φ and a fixed ampere–turn ratio $\hat{\Theta}_d/\hat{\Theta}_b = 2$.

Therefore, if $J_{c,i,rms} \leq J_{max}$ shall be maintained in all coils, the minimum volume V_{min} is given at $\varphi = 3\,\pi/4$, which has to be set by orientating the outlet of the pump accordingly. For the case shown in Fig. 12 ($\Theta_d/\Theta_b = 2$), this leads to a small volume reduction by $7\,\%$ as compared to the separated coils. At the same time, the copper losses are increasing slightly, as it is depicted in Fig. 13.

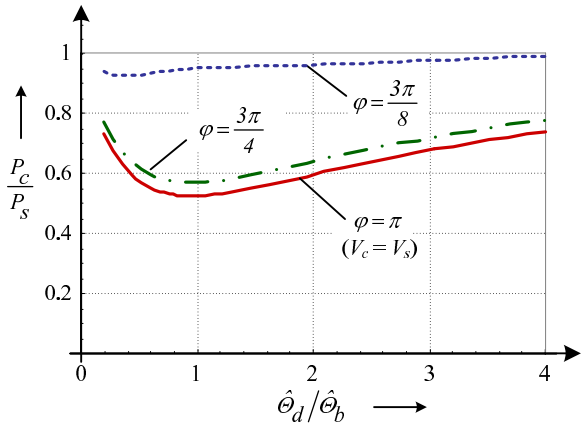

Fig. 13: Copper loss ratio for different load angles φ (and therefore different coil volumes according to Fig. 12) and $k_{lm} = 0.9$.

Hence, as long as the current density condition is kept, there is only an insignificant volume decrease possible. An interesting point is if locally higher current densities at some

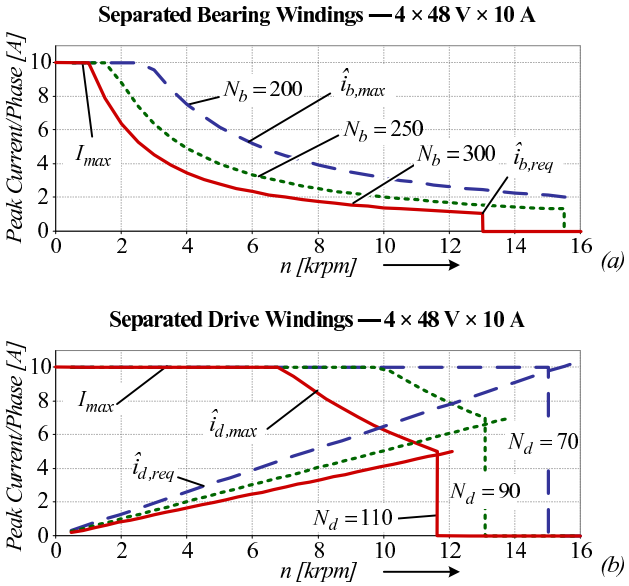

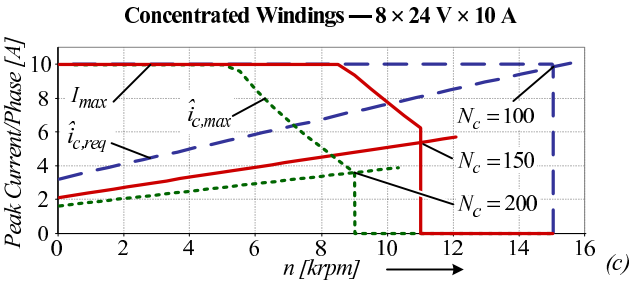

Fig. 14: Maximum achievable current and speed for separated bearing (a), drive (b) and concentrated coils.

coils are allowed (e.g. due to a good thermal coupling with coils with lower current densities) and the mean value of the current densities in the coils is kept below the maximum allowable value, i.e. $1/8 \sum_{i=1}^{8} J_{c,i,rms} < J_{max}$. The load angle φ that has to be set in order to achieve this point is in the area of $\pi/2 \ldots \pi/3$ (cf. Fig. 12) depending on the ampere–turns ratio Θ_d/Θ_b. As can be seen in Fig. 13, e.g. for $\varphi = 3\,\pi/4$ the total copper losses (in all concentrated coils) are approximately equal the copper losses of the separated coils, while the volume is reduced to about 70 % (area of local current density exceedence in Fig. 12). However, this also means a smaller heat sink volume, which may complicate the thermal situation in addition to the unequal current distribution, wherefore a thermal modeling of the system is indispensable in that case.

V. Power Electronics Requirements

For estimating the needed power electronics volume the *components load factor (CLF)* calculation [12] can be used. This factor is an indicator for size, costs and appearing losses in a system [12]. Two systems with the same *CLF* factor can be compared directly. According to [12], the power electronics approximately scales with $CLF \propto U^* \cdot I^*$. Of course, this factor does neither consider the effort for additional circuitry (such as gate driver circuits) nor it is based on a detailed loss analysis. However, is serves as a rough indicator for the total power electronics effort.

As mentioned before, the concentrated winding setup requires eight full–bridges while the separated coils require only four full–bridges. Therefore, in order to achieve the same *CLF*, either U_{DC} or I_{max} has to be doubled for the separated setup. With this, exemplarily possible combinations are given in Table I for $U_{DC} = 24\,V/48\,V$ and $I_{max} = 5\,A/10\,A$. The same component ratings are used for bearing and drive in case of separated coils even though the bearing requirements would permit lower current ratings.

Hence, regarding the power electronics requirements the two winding concepts are equivalent, as long as the same *CLF* is chosen in the design. As will be shown in the next section, the equality of the *CLF* leads to a fair comparison, since it means the same power being delivered to the motor.

Low power equal setups	
Separated coils	$4 \times 24\,V \times 10\,A$
Separated coils	$4 \times 48\,V \times 5\,A$
Concentrated coils	$8 \times 24\,V \times 5\,A$
High power equal setups	
Separated coils	$4 \times 48\,V \times 10\,A$
Concentrated coils	$8 \times 24\,V \times 10\,A$
Concentrated coils	$8 \times 48\,V \times 5\,A$

TABLE I: Possible power electronics setups with same *CLF*

VI. Maximum Achievable Rotation Speed

A. Separated coils

For a stable operation it has to be ensured that the minimum required bearing current given by $i_{b,req} = \Theta_{b,req}/N_b$ for a chosen number of windings N_b per coil can be impressed into the bearing coils at any time. The maximum applicable current in a coil is given by

$$\hat{i}_{b,max} = \frac{-\hat{u}_{ind} \cdot R \pm \sqrt{(R^2 + \omega_{el}^2\,L^2)\,U_{DC}^2 - \omega_{el}^2\,L^2\,\hat{u}_{ind}^2}}{R^2 + \omega_{el}^2\,L^2}, \tag{18}$$

which is a function of the induced voltage $\hat{u}_{ind}$, the total bearing phase inductance $L \propto N_b^2$, the supply voltage U_{DC} and the angular frequency $\omega_{el} = 2\,\pi\,n/60$, where n is the rotation speed in rpm. A stable operation of the bearingless motor with separated coils is therefore given for the condition $\hat{i}_{b,req} < \hat{i}_{b,max}$. For the separated coils, where no induced voltage is appearing in the bearing phase ($\hat{u}_{ind} = 0$, cf. section II), the maximum achievable current $\hat{i}_{b,max}$ is approximately decreasing with $1/n$ and limited by I_{max} given by the power electronics.

Fig. 14(a) shows the curves of the available peak currents per phase for different winding numbers N_b and for $U_{DC} = 48\,V$ and $I_{max} = 10\,A$. It can be seen that for lower number

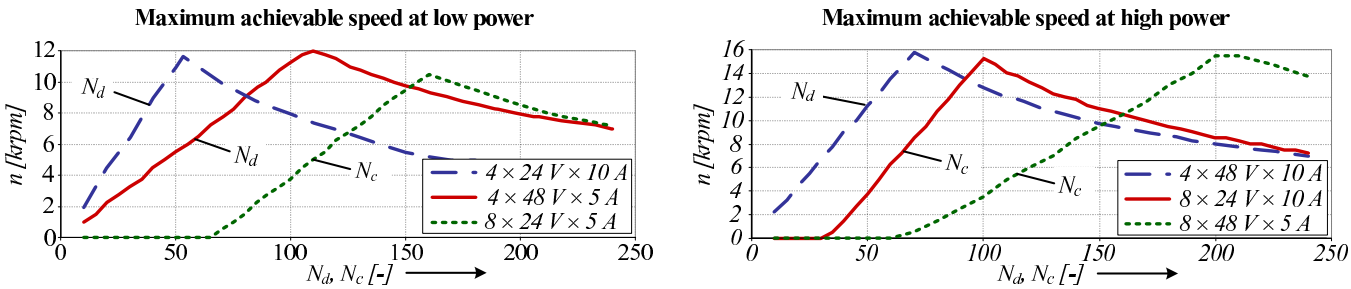

Fig. 15: Maximum achievable speed dependent on number of turns for low power (left picture) and high power (right picture).

of turns higher rotation speeds are feasible, but higher currents are needed and therefore higher losses in the power electronics occur. Additionally, it has to be ensured that the minimum needed drive current $\hat{i}_{d,req}$ can be impressed at any time. Analogously to (18), $\hat{i}_{d,max}$ can be calculated leading to the condition $\hat{i}_{d,req} < \hat{i}_{d,max}$. In case of a pump usually the drive requirements are more restrictive than the bearing ones. The pump performance is measured by the hydraulic pressure at a certain flow rate $Q = const$. Based on the scaling properties of pumps the pressure is scaled with

$$Y \quad \propto \quad n^2. \tag{19}$$

Therefore, a high rotation speed n is desireable in order to increase the hydraulic pressure and the power $P_{hyd} = Y \cdot Q$ of the pump.

However, also the drive current requirements are increasing with high rotation speeds according to

$$\hat{i}_{d,req} \propto M = \frac{P}{n \cdot 2\,\pi/60} \propto n. \tag{20}$$

Out of this requirement the minimum needed current $\hat{i}_{d,req}$ can be calculated. Curves for three different winding numbers are plotted in Fig. 14(b). The maximum achievable rotation speed is given by the crossing of the $\hat{i}_{d,req}$ and the $\hat{i}_{d,max}$ curves, which are both dependent an the number of turns N_d.

B. Concentrated Coils

Due to $\Theta_c = \Theta_b + \Theta_d$ in case of concentrated coils the condition

$$\hat{i}_{c,req} \cdot N_c = \hat{i}_{b,req} \cdot N_b + \hat{i}_{d,req} \cdot N_d < \hat{i}_{c,max} \cdot N_c \tag{21}$$

has to be satisfied. Therefore, the minimum needed current $\hat{i}_{c,req}$ is a superposition of the minimum needed bearing ampere–turns and the minimum needed drive ampere–turns with (20). The needed bearing current is almost independent of the rotation speed and is causing the offsets in the current curves in Fig. 14(c), which are plotted for a *CLF* equivalent system as compared to Fig. 14 (a)/(b). Due to the superposition of the drive and bearing ampere–turns the required current $\hat{i}_{c,req}$ is now higher than for the separated case (cf. Fig. 14(a)/(b)).

Thus, the maximum achievable speed is depending on the winding numbers, which is shown in Fig. 15 for both separated and concentrated coils for the load cases mentioned in section V. Since the bearing system is not the limiting factor in case of separated coils, only the dependency of the maximum achievable speed on the drive winding number N_d is plotted.

One can see that especially at low power (left picture in Fig. 15) with separated coils higher rotation speeds can be achieved. The main reason for this is that there is no induced voltage appearing in the bearing phase and therefore only the needed drive current has to be built up against the induced voltage. At high power (right picture in Fig. 15) this benefit disappears and approximately the same maximum speed can be achieved with both winding concepts.

VII. Conclusions

In this paper two different winding concepts for bearingless pumps have been discussed. The comparison was based on the assumptions of the same needed force and torque in both cases, same dimensions, same iron circuit, same magnet size and magnetization, same maximum current density and finally the same winding factor in the coils. The concepts have been compared concerning the copper losses, the total coil volume, the maximum achievable speed and the requirements for the used power electronics.

A qualitative compilation of the results is given in Tab. II. The most remarkable difference between the two concepts is the aspect of the copper losses, where a realistic reduction of about 30 % can be achieved for the concentrated coils. Regarding the coil volume, there is a general trade–off between the coil volume and the copper losses, i.e. a smaller volume will always lead to higher losses. However, if the maximum current densities in all coils shall not be exceeded, there is no significant volume decrease possible for the concentrated coils. If local exceedence of current densities is allowed in some claws (and the mean value of the current densities is still below the maximum allowable current density), the volume can be reduced to about 70 %. However, in this case the benefit of the loss reduction for the concentrated coils is lost and the coil losses are equal for the both cases.

The calculations for the volume and loss comparison are based on the assumption of sinusoidal bearing and drive currents and a load angle φ, which is occurring between the bearing and the drive currents and is dependent on the orientation of the outlet of the centrifugal pump. In an experimental setup (cf. Fig. 17) these assumptions have been validated for two outlet configurations (cf. Fig. 16)

Basically, for the concentrated coils twice the number of

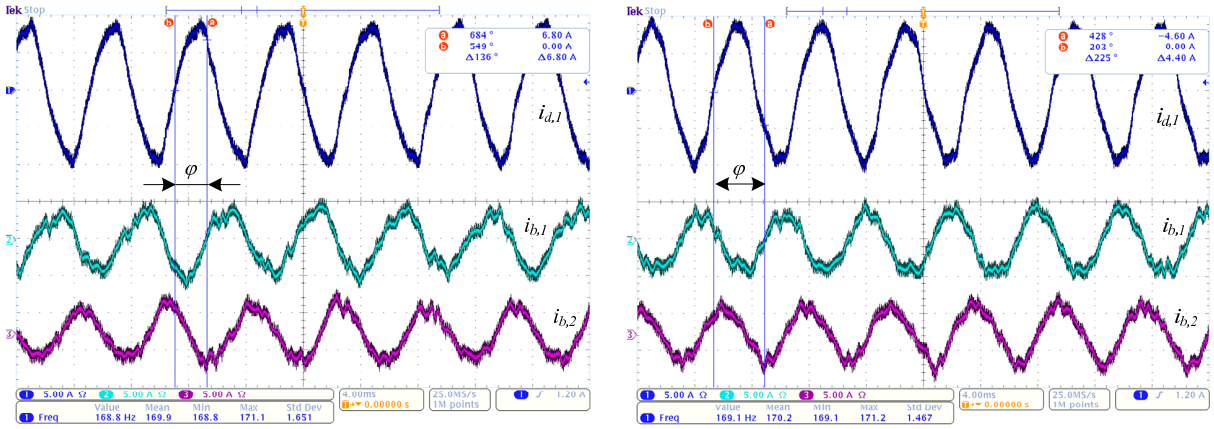

Fig. 16: Current measurements for two outlet configurations (left: $\varphi = 3\,\pi/4$, right: $\varphi = 5\,\pi/4$) at 10'000 rpm, $14\,l/min$ hydraulic flow rate and $1.6\,bar$ outlet pressure. (Current scale $5\,A/div$, time scale $4\,ms/div$)

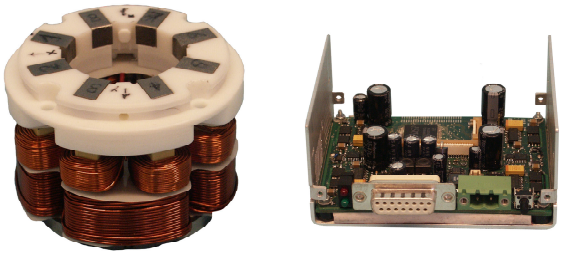

Fig. 17: Experimental setup with separated coils and power electronics with four full bridge inverters.

	Sep. coils	Conc. coils
Copper losses	−	+
Coil volume	✓	✓
Power electronics	✓	✓
Maximum speed	+	✓
Manufacturability	✓	+
Control effort	✓	−
Cabling effort	✓	−

TABLE II: Comparison of separated and concentrated winding concepts

full–bridges is required. However, if the same power shall be delivered to the pump in order to perform a fair comparison, the concentrated coils can be driven with either half the current or half the voltage. This leads, in consequence, to approximately the same power electronics requirements.

Regarding the maximum achievable speed the two concepts show similar performance for high power delivered to the pump (e.g. $48\,V/10\,A$ for the separated coils and $24\,V/10\,A$ for the concentrated coils). For lower power (e.g. $48\,V/5\,A$ for the separated coils and $24\,V/5\,A$ for the concentrated coils) the maximum achievable speed is noticeably lower in the case of concentrated coils. This is due to the fact that the induced voltages are appearing in all concentrated coils and are reducing the coil voltages (in case of separated coils the induced voltages are not present in the bearing system due to the winding configuration).

As to manufacturability, there is an apparent advantage for the concentrated coils, both in terms of number and uniformity. On the other hand, the calculation and control of the eight required currents leads to a clearly higher effort for the concentrated coils. Finally, also the cabling effort has to be taken into account, which is doubled for the concentrated coils.

Therefore, the decision about the preferable winding concept has to be taken from case to case depending on the application, since both concepts have their advantages in different aspects. However, for given specifications, the calculations and considerations detailed in this paper can serve as a guideline for the selection of the appropriate winding concept.

REFERENCES

[1] M. Neff, "Bearingless pump system for the semiconductor industry," in *6th International Symposium on Magnetic Suspension Technology*, 2001, pp. 169–173.

[2] ——, "Bearingless centrifugal pump for highly pure chemicals," in *Proc. 8th ISMB*, Aug. 2002, pp. 283–287.

[3] "Levitronix website," 2007. [Online]. Available: http://www.levitronix.com/

[4] T. Nussbaumer, K. Raggl, P. Boesch, and J.W.Kolar, "Trends in integration for magnetically levitated pump systems," in *PCC Nagoya*, 2–5 April 2007, pp. 1551–1558.

[5] N. Barletta, "Der lagerlose scheibenläufer," Ph.D. dissertation, Electrical Engineering and Design Laboratory, ETH Zurich, 1998.

[6] R. Schoeb, "Principle and application of a bearingless slice motor," *JSME International Journal*, vol. 40, no. 4, pp. 593–598, 1997.

[7] G. Schweitzer, "Active magnetic bearings — chances and limitations," *6th International Conference on Rotor Dynamics*, pp. 1–14, Oct. 2002.

[8] J. Bichsel, "The bearingless electrical machine," *International Symposium on Magnetic Suspension Technology*, vol. 2, pp. 1–14, Aug. 19–23 1991.

[9] S. Silber, W. Amrhein, P. Bösch, R. Schöb, and N. Barletta, "Design aspects of bearingless slice motors," *IEEE/ASME Transactions on Mechatronics*, vol. 10, no. 6, pp. 611–617, 2005.

[10] W. Amrhein, S. Silber, and K. Nenninger, "Levitation forces in bearingless permanent magnet motors," *IEEE Transactions on Magnetics*, vol. 35, no. 5, pp. 4052–4054, 1999.

[11] M. Takemoto, M. Uyama, A. Chiba, H. Akagi, and T. Fukao, "A deeply–buried permanent magnet bearingless motor with 2–pole motor windings and 4–pole suspension windings," in *Conference Record of the 38th Industry Applications Conference (IAS)*, vol. 2, 2003, pp. 1413–1420.

[12] B. Carsten, "Converter component load factors; a performance limitation of various topologies," in *PCI*, June 1988, pp. 31–49.